Ceramics-Silikáty 63 (3), 277-286 (2019)
www.ceramics-silikaty.cz doi: 10.13168/cs.2019.0021

BITUMINOUS COMPOSITE COMPRISING AMORPHOUS SILICA FROM RICE HUSKS

#SIMON SEMBIRING*, AGUS RIYANTO*, RUDY SITUMEANG**, ZIPORA SEMBIRING**

*Department of Physics, Faculty of Mathematics and Natural Sciences, Lampung University, Jl. Prof. Soemantri Brojonegoro No.1 Bandar Lampung, 35145, Indonesia
**Department of Chemistry, Faculty of Mathematics and Natural Sciences, Lampung University, Prof. Soemantri Brojonegoro, No 1 Bandar Lampung, 35145, Indonesia

#E-mail: simonsembiring2@gmail.com

Submitted March 14, 2019; accepted accepted May 6, 2019

Keywords: Rice husk, Silica, Asphalt, Microstructure, Structure

The composites were prepared with a ratio of bitumen to silica of 1:0, 1:1.5, 1:1.6, 1: 1.7, 1:1.8, 1:1.9 and 1:2 by weight, and calcined at the temperature of 150 °C for 6 hours. The structural and microstructural characteristics of the bituminous composites were examined by X-ray diffraction (XRD), Fourier Transform Infrared (FTIR), Differential Thermal Analysis (DTA/TGA), and Scanning Electron Microscopy/Energy-Dispersive X-ray (SEM/EDX). Further evaluation was made by comparing the characteristics of the modified bituminous composites including the density, porosity, compressive strength, swelling thickness, and water absorption. The XRD study revealed that the major phases were silica and carbon amorphous, which were associated with the Si–OH, Si–O-Si and C–H functional groups according to the FTIR analysis. The DTA/TGA analysis resulted in an increase in the temperature decomposition by adding silica which was 230 to 315 °C. In addition, an increased silica addition was followed by an increase in the density, compressive strength, swelling thickness, and water absorption, while the opposite was true for the porosity. Based on these characteristics, rice husk silica has a positive effect on improving the mixture of high and low temperature performance, water stability, for use as a substitute in lightweight steel roof devices.

INTRODUCTION

The present study was carried out with the aim of exploring the feasibility of rice husk silica to produce asphalt composite precursors for roofing materials. Rice husk silica was chosen because of the high availability of rice husks as an agriculture residue, which makes it a cost-effective alternative as a silica source. Based on several studies, the potential of rice husks was investigated in recognition of its high purity and reactive silica [1-2], and the solubility of the silica in an alkaline solution, thus enabling the production of rice husk silica in the form of sols. In addition, rice husk silica is known as a porous and high-grade amorphous material [3-7], which has the potential to become a suitable raw material for the production of various silica-based materials, such as the production of a nano-silica [1, 8-9], zeolite [10-12], mullite [13-14], forsterite [15-16], nepheline [17] and cordierite [18].

Due to its excellent stability, the high surface area, strong adsorption, and good dispersing ability, silica also has the potential to help prepare asphaltic materials with desirable properties. For example, Sarsam, 2013 [19] observed that the viscosity and the softening point of asphalt increased significantly with increased silica fumes from 1 to 4 %, while from 1 to 2 % the penetration value decreased, the elastic strain and temperature susceptibility increased [20]. Mojtaba et al., 2012 [21] observed that when 2 % of SiO_2 was added to asphalt mixes, it caused increased mechanical behaviour. The bitumen (asphalt) resistance's ability to deform the stability can be obtained by using 7 % silica based on the asphalt weight [22], while Yao et al., 2012 [23] used 4 and 6 % silica to modify the asphalt. They concluded that resistance to ageing and fatigue cracking increased. In a previous study [24], the investigation was conducted to modify asphalt using clay and reported that asphalt thermal stability increases, while asphalt mixed with montmorillonite and carbon can decrease the asphalt inertia and increase the hardness [25].

Bitumen is a hydrocarbon compound comprised of 80 % carbon, 10 % hydrogen, 6 % sulfur and remaining percent made from nitrogen and oxygen. In addition to the increased concentrations of C=O groups, photooxidation may lead to the increased presence of certain types of sulfur-oxygen groups, including sulfate groups (SO_4), thus, leading to the hardening and embrittling of the asphalt [26-27]. Besides, with heat treatment, the asphalt transforms into an adhesive liquid and easily mixes with other materials. In the process of cooling, the asphalt becomes waterproof, adhesive and strong. While adding a functionalised polymer to asphalt, specific interactions, such as hydrogen bonding, can be observed between the

asphalt and the polymers. Also, some other forms of chemical reactions could take place between the reactive groups of the matrix (asphalt and polymers).

Bitumen is one of the most potentially used products for roofing materials due to the aggregation of the binders. This is because of the adhesive, high viscoelastic and chemical resistance properties [28-29]. Unfortunately, due to severe temperature susceptibility, its applications are limited. Therefore, necessary modifications are required. Several materials have the possibility to be utilised along with asphalt, such as hydrated lime, plastic powders or polymerised powders. Previously, several studies have been conducted to modify and improve the characteristics of the asphalt such as using a natural liquid rubber [30] and a natural rubber latex [31]. Some researchers have also tried to change the characteristics of the asphalt to improve its functionality and benefits by using various polymers like styrene–butadiene–rubber [32], crumb rubber [33], waste tire rubber [34], fibres and waste fibres [29, 35], and a polymeric nanocomposite [36-37]. Not only does it have good durability, abrasion resistance, and resistance to crack deformation using a modified asphalt pavement, but it can also maintain good stability at high- or low temperatures [38-39]. In addition, modified asphalt waterproofing materials have excellent imperviousness, therefore, it has more applications in the building waterproofing material industry [40-41]. With the addition of other particles, the cohesion and viscosity of the asphalt may increase, which are good for high-temperature conditions [42].

This work was undertaken with the aim of investigating the structural and microstructural properties of asphalt with the addition of silica from rice husks and to know its relation to the physical properties of the asphalt composites for roofing materials. This work has emphasised the influence of variations of the relative silica content to the asphalt on the structural, microstructural and physical properties of asphalt composites prepared from amorphous rice husk silica. XRD, FTIR, DTA/TGA and SEM/EDX were used to obtain detailed information about some asphalt characteristics with the addition of the silica. Furthermore, the physical properties of the asphalt composites are investigated by measuring the density, porosity, compressive strength, water absorption and swelling thickness.

EXPERIMENTAL

Materials

The silica feedstock is taken from rice husks and the chemicals used are 5 % NaOH 5 % KOH, 5 % HCl, and absolute alcohol (C_2H_5OH) purchased from Merck (kGaA, Darmstadt, Germany), and distilled water. An asphalt obtained from the Buton refinery, Southeast Sulawesi Province, Indonesia was used in the present investigation.

Procedure

The bituminous composite synthesis is carried out with the following steps, (i) extraction of the silica, (ii) synthesis of the bituminous composites with different additions of silica.

Extraction of the silica

Rice husks were used to extract and obtain the silica by following the literature in previous studies [15]. The sol obtained is dripping with a 5 % HCl solution until the sol turns completely into a gel. The gel was dried at 110 °C for eight hours and then ground into a powder by mortar and sieved to a 200 mesh.

Synthesis of the bituminous composites

Synthesis of the bituminous composite was carried out with a precise mixture of bituminous and silica mass. Typically, 50 g of solid bituminen is melted by heating at 100 °C and mixed with the powdered silica using a shear mixer at a rate of 125 rpm for 4 hours. To obtain the bituminous composite, the calculated quantity of the silica is added under stirring to the asphalt to provide the bitumen to silica ratio with a mass ratio of 1:0, 1:1.5; 1:1.6; 1:1.7; 1:8; 1:1.9 and 1:2. Furthermore, the powder was pressed into the form of a cylinder pellet with a pressure of 2×10^4 $N \cdot m^{-2}$. The pellet is then calcined at 150 °C for 6 hours.

Characterisation

The collection of the XRD data was conducted with an automated Shimadzu XD-610 X-ray diffractometer at the National Agency for Nuclear Energy (BATAN). The XRD data was taken with CuKα radiation (λ = = 1.5406 nm) at 40 kV and 30 mA in the range of 2θ = = 5-80°, with a step size of 0.02, counting time 1 s/step and a 0.15° receiving slit. The FTIR data was taken with a Perkin Elmer FTIR. The sample was prepared by mixing with KBr of spectroscopy grade. The microstructural analysis of the polished and etched samples was undertaken by SEM Philips-XL. The thermal analysis was performed using a DTA Merck Setaram Tag 24 S, under a nitrogen atmosphere with a constant heating rate of 3 °C/min, at the temperature range of 30 to 800 °C. Archimedes' method was used to measure the bulk density and apparent porosity [43]. The water absorption and swelling thickness were measured in accordance with JIS A 5908 [44]. The compressive strength was determined with three replicate measurements following ASTM C268-70.

RESULTS AND DISCUSSION

Characterisation of the asphalt composite with different silica additions

The structural transformation of the samples was performed using XRD and the results are shown in Figures 1a-g. Figure 1a shows the spectrum of the bitumen without the addition of the silica and Figures 1b-g show the spectra of the samples with the different silica additions. The diffraction peak intensity of the sample without the silica addition (Figure 1a) was found at approximately 18-25° and 40° values of 2θ, amorphously indicating it came from crystalline asphaltenes, as demonstrated by the previous study [45-46]. The peak asphaltene appears at about 2θ = 20° (Figure 1a), due to the aliphatic chain and forms an aromatic stack of molecules under the influence of London's dispersion forces. The aliphatic chain represented in asphaltene is known as multilayer graphene which extends from the central aromatic part of the asphaltene molecule [47-48]. At the 2θ value (43.12°), a weak bond is formed, which is due to the influence of nearest neighbours in the ring structure [49].

Similarly, the diffraction peak intensities of the samples with the addition of the silica were found to be 10 and 21.8° (Figures 1b-g), amorphously indicating the background intensities from the carbon and silica, representing the amorphous scatter. The presence of an amorphous phase is presumably indicative of the silica and carbon accumulating on the surface. However, the change in the peak diffraction is a result of strong molecular interactions between the bituminous and the silica through the exfoliation and intercalation process in the samples. This may indicate that there are many interactions in the form of crystallisation that do not separate the asphaltene molecules outside their range of London attractions between the silica and bituminous. This result also shows that the intercalation and peeling occur as evidenced by the modified bitumen peaks falling between the two peaks associated with the carbon and silica. This, in turn, suggests an increasing layer distance due to the modification.

To investigate the formation of the functionality and follow the dehydration reaction with the addition of rice husk silica, the samples were characterised by FTIR. The FTIR spectra of the samples with different rice husk silica are demonstrated in Figures 2a-g. Figure 2a presents the infrared spectrum of the bitumen without the addition of rice husk silica and Figure 2b-g presents the phase peak intensities of the samples with different silica additions. For the bituminous sample without silica (Figure 2a), the high peak appeared at 1752 cm^{-1}, which indicates the vibration of the carbonyl C=O group. In addition, the attendance of the peaks at 958, 816, and 749 cm^{-1} corresponds to the bending vibration of C–H in a phenyl, as supported by a previous study [50]. Other observed strong bonds located at 2938 and 1474 cm^{-1} may show the characteristic group functionality of O–H from carboxylic acids and C–H from alkanes.

The obvious effect with the addition of the silica to the functionality of the samples is shown in Figure 2b-g. The significant influences are the emergence of a related peak with hydroxyl functionality at around 3709 cm^{-1},

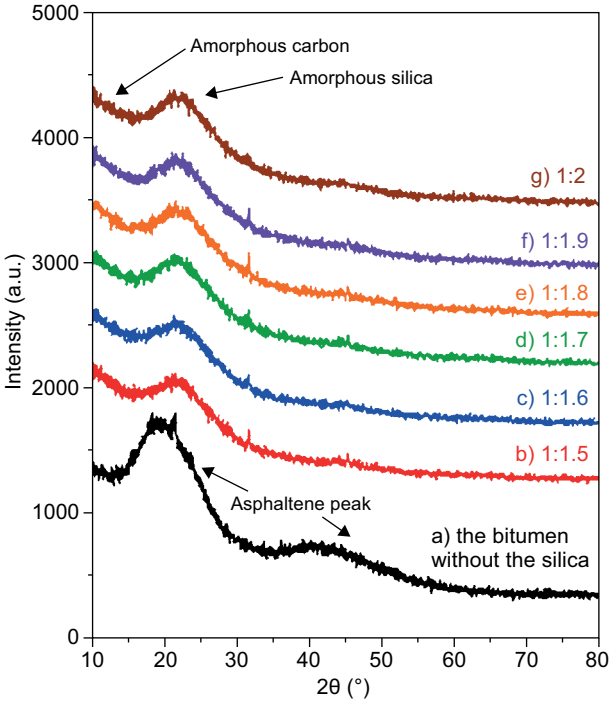

Figure 1. The X-ray diffraction patterns of the samples with the different ratios of bitumen to silica using CuKα radiation.

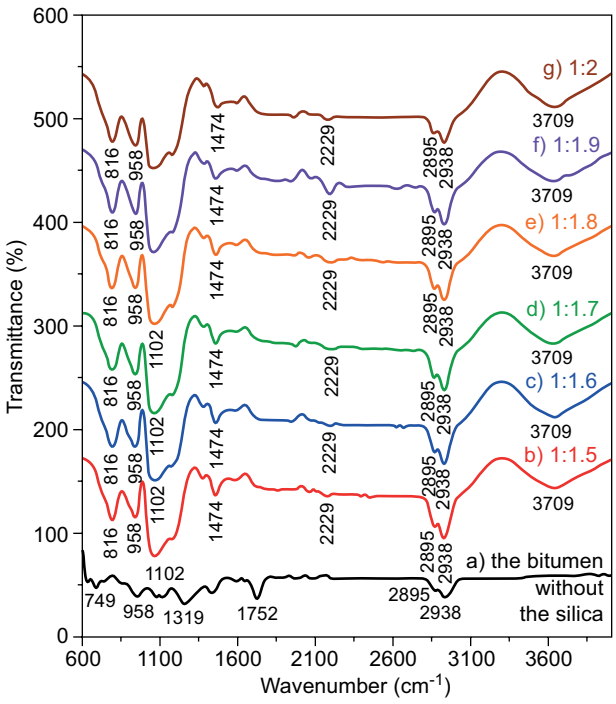

Figure 2. The FTIR spectra of the samples with the different ratios of bitumen to silica.

which indicates the reaction between silica and bitumen during the silica addition process. As confirmed in previous research [51], shows that the O–H absorption bonds are derived from silanol in $Si(OH)_4$ produced by the vibration of H–OH. The appearance of Si $(OH)_4$ is shown in the absorption wave number 1102 cm^{-1}, which indicates that the Si–O–Si bond formed by the deformation of the Si-O vibration, as has been observed by Tsai, 2002 [52]. The presence of SiO vibration is observed in the results, showing the strong non-bonded interaction of the SiO tetrahedra with bitumen. In other words, the SiO vibration also suggests both distortions in the SiO tetrahedra and stronger interactions between the asphalt and silica. Other observed strong bonds are located at 1474 and 2938 cm^{-1} and possibly show the characteristic functionality of O–H from carboxylic acids and aliphatic [50, 53], and C–H from alkanes, respectively [54-55]. The bond of C–H replaced by butadiene (ethylene bond) is located at the peak of 958 cm^{-1}. Based on the results of the chemical bond analysis, the addition of silica shows the peak chemical bond change of the bitumen. Also, it can be informed that the bitumen undergoes changes between its bonds and the silica.

The thermal characteristics of the samples were evaluated by analysing the samples with TGA/DTA. The TGA thermograms of the samples with different rice husk silica additions are compiled in Figure 3 and the DTA thermograms are shown in Figure 4. Figure 3a is the TGA of the sample without the silica addition, showing a very small weight loss at around 230 °C and a very large weight loss occurs up to 453 °C. The DTA thermogram of the bituminous sample without the silica (Fig. 4a) shows the existence of two endothermic peaks located at around 100 and 450 °C, and one exothermic peak located at around 480 °C. The peak in the range of 100 °C is most likely due to the evaporation of water and the residual organics probably present during the preparation of the samples. The peaks at around 450 and 480 °C could be assigned to the dehydration of asphaltene molecules, as supported by the XRD results in Figure 1a.

The thermal gravimetric analysis method was used to determine the weight loss of the samples with the curve of the temperature and to determine the samples temperature stability. The TGA thermograms of the samples with the addition of the silica (Figures 3b-g) have undergone two major weight loss stages. The first stage, a very small weight loss (Figures 3b-g and Table 1) occurs in the temperature range of 30-300 °C, and the weight loss of sample is mainly due to the removal of water and the volatility of the asphaltene components such as the saturation and decomposition of asphaltene

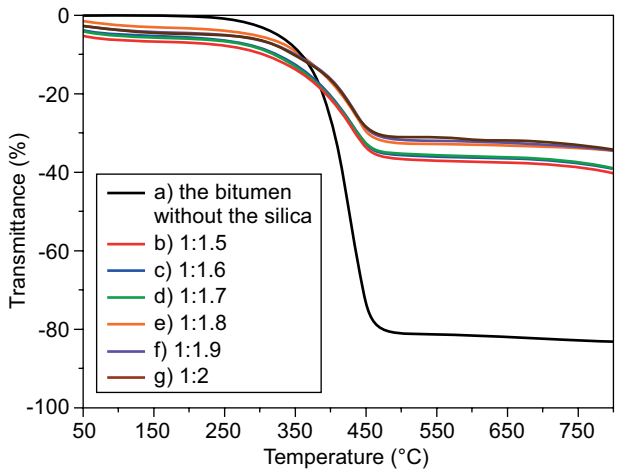

Figure 3. The TGA thermograms of the samples with the different ratios of bitumen to silica.

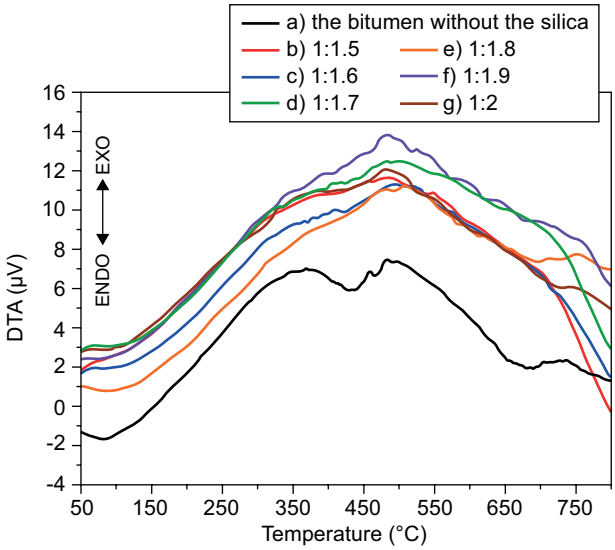

Figure 4. The DTA thermograms of the samples with the different ratios of bitumen to silica.

Table 1. Summary of TGA properties results for all samples.

Sample	Onset temperature (°C)	Max. temperature (°C)	Weight loss (%) 30-300 °C	Weight loss (%) 300-500 °C	Residue after 500 °C (%)
Asphalt	230	453	-0.5	-79.9	20.6
1:1.5	233	459	-6.4	-36.4	57.2
1:1.6	267	463	-6.7	-35.6	57.7
1:1.7	272	470	-7.2	-34.9	57.9
1:1.8	283	473	-4.4	-30.8	64.3
1:1.9	288	477	-5.6	-30.1	64.5
1:2	315	497	-5.9	-29.3	64.8

[56]. In this stage, DTA thermograms (Figures 4b-g) revealed a small endothermic peak located at around 100 °C. The second step, the weight loss starts at 300 °C and ended at 500 °C, the results show a very sharp weight loss. The weight loss was mainly attributed to the further volatilisation of the decayed residues of the asphaltene decomposition and silica crystallisation, supported by the endothermic peak presence at around 500 °C in the DTA thermograms as shown in Figures 4 b-g. From 300 to 500 °C, the rate of the weight loss decreased sharply as the temperature increases, and after 500 °C, the samples, practically have reached a stable state, the TGA curve became flat as displayed in Figure 3 b-g. This means that the silica particles and asphalt mixed homogeneously to form a compact blend. Compared to the weight loss of the asphalt without the silica and the asphalt with the addition of the silica (Table 1), the amount of asphalt without the silica is 79.9 % to 500 ° C, while the amount of the silica addition from 1.5 to 1.7 g of weight loss decreases from 36.4 to 34.9 %, and an increase in the number of silica additions from 1.7 to 2 g, weight loss decreased from 34.9 to 29.3 %. These results indicate an increase in the temperature stability along with the addition of the silica. The TGA results showed that the sample performance, such as viscosity, tensile strength, and high temperature stability, had increased significantly with the addition of the rice husk silica. That is due to the strengthening the interface interaction between the silica and the bitumen.

The surface images of the samples with the different ratio of bituminous to silica obtained from the SEM analyses are shown in Figure 5a-g and followed by the chemical composition as shown in Table 2. Examination of the SEM micrographs presented in Figure 5a-g shows the reaction between the silica and bituminous on the sample surface. The microstructure of the sample without the silica addition (Figure 5a) shows a quite different characteristic, in comparison with the addition of 1.5 g and 1.6 g of the silica (Figures 5b and c). The image in Figure 5a indicates the existence of clusters with a large size, most likely deriving from the arrangement of asphaltenic structures. The microstructures of the samples prepared at ratios of 1:1.5 (Figure 5b) and 1:1.6 (Figure 5c) do not show any major difference. The surfaces of both samples are characterised by smaller silica particles that cover several large grains of the asphaltenic structures. The silica reacts with the bitumen, so the particle size of the silica becomes smaller, as the silica crystallinity rate increases. Both samples were followed by the initial coalescence of the silica and bituminous. These changes are presented in the XRD results for the samples with the addition of the silica in Figure 3b-c, in which the silica was detected. As shown by the SEM examinations in Figure 5d-g, it indicated that the surface profiles at higher ratios of 1:1.7, 1:1.8, 1:1.9 and 1:2 are distributed homogeneously in the form of porous deposits in the asphaltenic structure and covered some small grains of silica. All the samples are marked by initiated as a high crystalline of silica, leading to the formation of the bituminous composite.

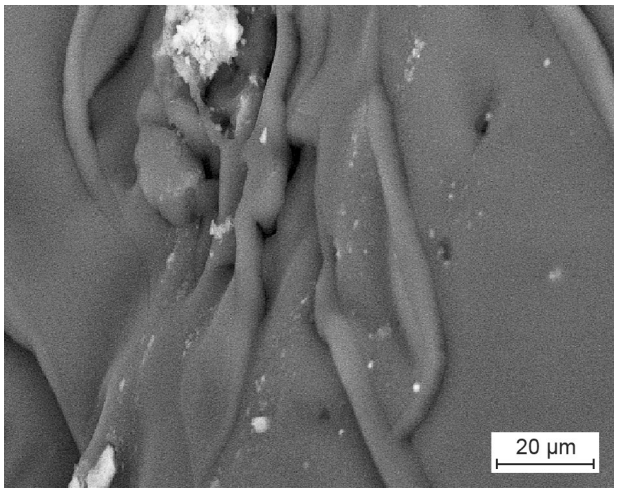

a) the bitumen without the silica

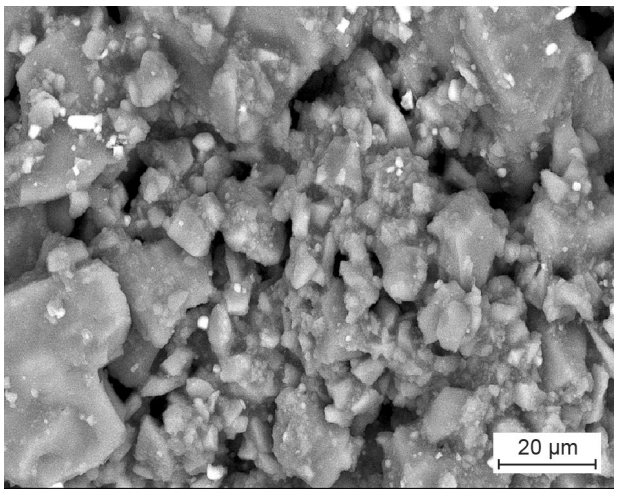

b) 1:1.5

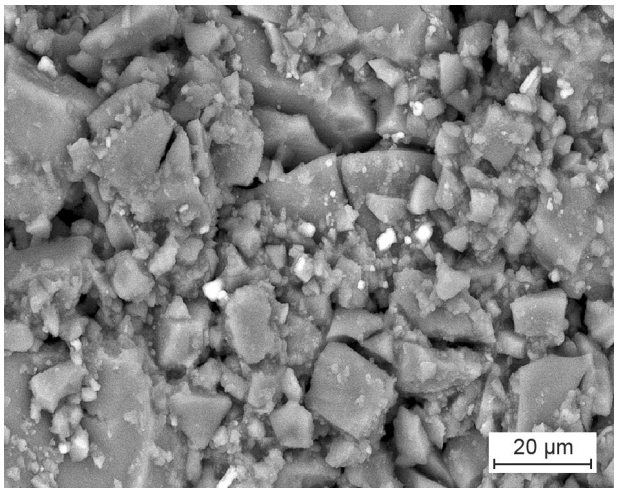

c) 1:1.6

Figure 5. The scanning electron microscopy (SEM) images of the samples with the different ratios of bitumen to silica. *(Continue on next page)*

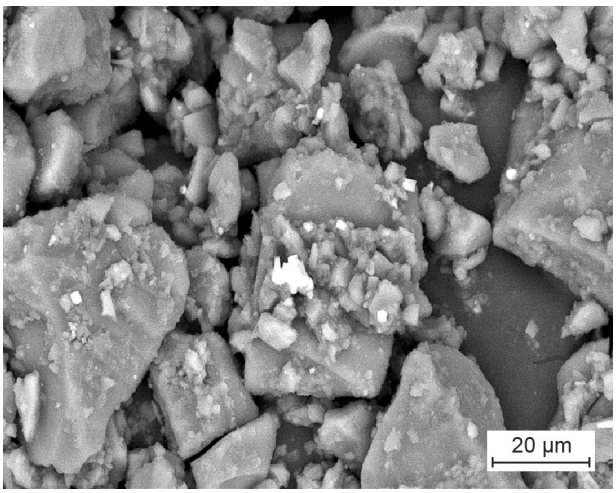

d) 1:1.7

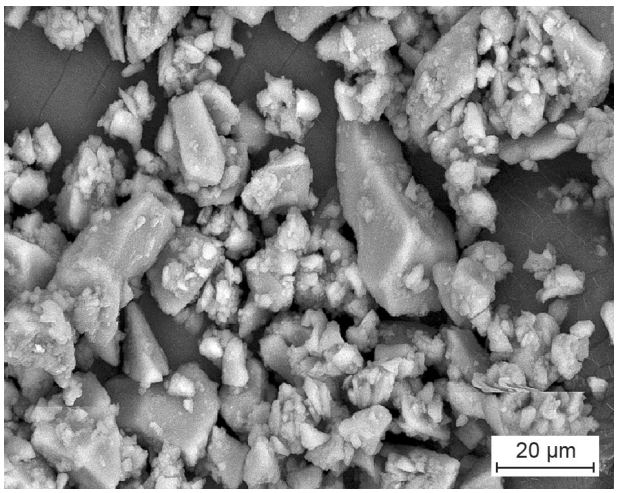

e) 1:1.8

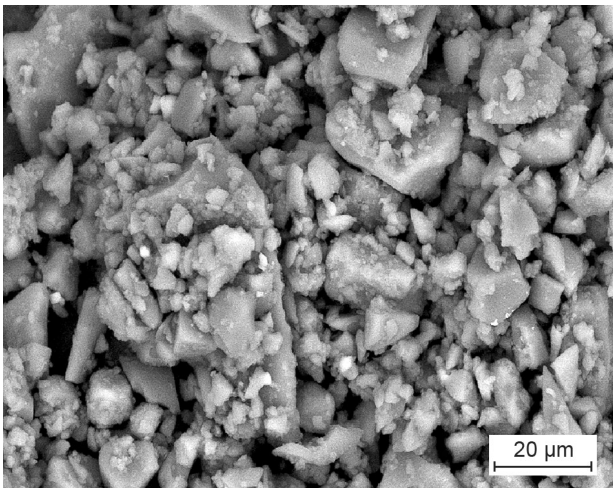

f) 1:1.9

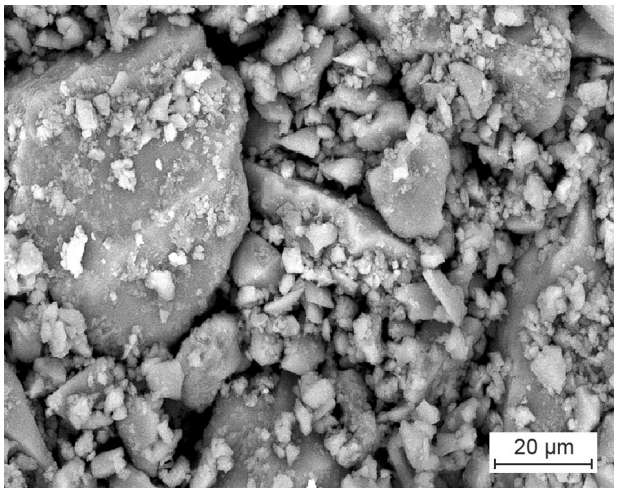

g) 1:2

Figure 5. The scanning electron microscopy (SEM) images of the samples with the different ratios of bitumen to silica.

Table 2. Composition of samples according to EDX spectra.

Sample	Carbon (wt. %)	Na_2O (wt. %)	SiO_2 (wt. %)	SO_3 (wt. %)	Cl (wt. %)
Asphalt	91.77	–	–	8.23	–
1:1.5	68.86	1.70	25.14	3.48	0.82
1:1.6	63.64	2.86	28.47	3.47	1.56
1:1.7	63.30	3.08	28.98	2.99	1.64
1:1.8	61.54	0.89	34.05	3.26	0.27
1:1.9	56.00	1.44	38.49	3.36	0.70
1:2	53.19	1.22	41.66	3.59	0.34

Analysis of the composition data is demonstrated in Table 2. Table 2 obviously revealed the significant addition of the silica content relative to bituminous on the silica and carbon composition. As shown in Table 2, a high amount (91.77 %) of the carbon was obtained from the bitumen without the silica and this element was reduced to 53.19 % with the addition of the silica up to 2 g. Meanwhile, the sample with the silica addition of 1.5 g contained 25.14 % and increased to 41.66 % with the silica addition up to 2 g. Furthermore, the SEM image indicates that the sample is denser with the addition of 2 g of silica, which leads to a compact shape indicated by the TGA analysis (Figure 3 and Table 1).

Physical characteristics of the synthesised asphalt composite

Figure 6 represents the variation of the density and porosity with the addition of the silica. It is clear that the porosities of the samples increase sharply at the silica addition to 1.7 g and decrease sharply up to the 1.8 g addition (Figure 6a). Meanwhile, the densities of the samples decrease sharply at the silica addition to 1.7 g and increase sharply up to the 1.8 g addition. The increase in the porosity as the silica addition to 1.7 g is most likely caused by dominant carbon as shown in Table 1. As shown in Figure 6a, the porosities increase from 12.5 to 14.8 % as the silica content increases from 1.5 to 1.7 g. The porosity sharply decreased as the silica content increased from 1.7 to 1.8 and reached the value

of 10.8 % of the silica content of 2 g. The sharp decrease in the porosity with the increasing silica content up to 1.8 was attributed to the proportional amount of carbon and silica, whereas the addition of silica in higher quantities did not cause a remarkable decrease in the porosity (Table 1).

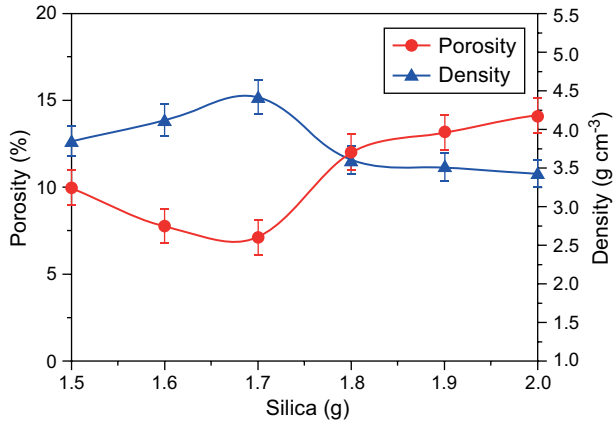

Figure 6. Variation in the porosity and density of the samples with the different silica additions.

The densities of the samples decrease sharply at the silica addition to 1.7 g and increase sharply up to 1.8 g, and the density slightly increased as the silica content increased from 1.8 to 2 g. As shown in Figure 6b, the densities decrease from 3.30 to 2.70 g·cm^{-3} as the silica content increases from 1.5 to 1.7 g. The density sharply increased as the silica content increased from 1.7 to 1.8 g and reached the value of 4.10 g·cm^{-3} at the silica content of 2 g. Increasing the silica content over 1.7 % seems to suppress the pore propagation inside the matrix, causing no abrupt porosity change to occur. Although the density increased in a small extent from the addition of 1.8 to 2 g silica, significant changes occurred in the density of these samples. This is due to the different densities of the carbon and silica, which caused the density to increase and the porosity to decrease. In other words, the decrease in porosity is due to the presence of the decreasing pore numbers of different sizes in the asphalt composite structure. This is also due to the presence of the carbon surrounding the silica particles and the decrease in the carbon by the addition of the silica. Furthermore, it is observed that the silica particles, as a reinforcement, have a tendency to bind themselves leading to the formation of groups of pores, which increase the numbers of homogeneous pore nucleation sites inside the bituminous composite structures.

The effect of the rice husk silica addition on the compressive strength is shown in Figure 7. The result indicates that the compressive strength of the bituminous composite increased with increasing rice husk silica content. As shown in Figure 7, the compressive strength increased sharply as the silica addition rose from 1.5 to 1.8 g. The sharp increase in the compressive strength with the increasing silica content up to 1.8 referred to the large decrease in the porosity and the increase in the density as shown in Figure 6. The compressive strength increased smoothly with the increasing silica form 1.8 to 2 g, and reached the value of 7.61 N·cm^{-2} at the silica content of 2 g. This trend implies that the samples became highly compact and dense as a result of the increased amount of silica and the decreased amount of carbon (Table 1). From a practical point of view, this finding demonstrates that the compressive strength of the samples is compatible with the change in the porosity and the density results in this study (Figures 6a and b). The role of the density and porosity in determining the compressive strength is in agreement with the structure profile of the samples as revealed by the XRD results (Figure 1). Other factors that control the compressive strength are probably both the homogeneity and the distribution of the particles, which is in accordance with the surface morphology of the samples, as shown in Figure 5.

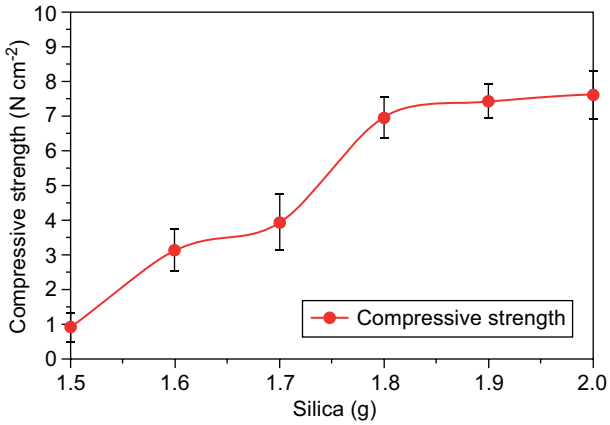

Figure 7. Variation in the compressive strength of the samples with the different silica additions.

The water absorption and swelling thickness of the bituminous composites made of the various rice husk silica additions are given in Figure 8. It can be clearly seen in Figure 8 that the water absorption and swelling thickness of all samples increased sharply from the silica content of 1.5 to 1.8 g, and was relatively flat up to 2 g. The increase in the water absorption and the swelling thickness with the increasing silica content up to 1.8 was attributed the proportional amount of carbon and silica (Table 1) and the presence of a number of microvoids caused by a larger number of poorly bonded areas between hydrophilic of silica and hydrophobicity of the bitumen. This shows that the water absorption and swelling thickness increase with the silica addition, until a certain value is attained, where it defined the water absorption and the swelling thickness. In other words, the possible reason is the reduced dispersion and interfacial adhesion between the bitumen and the silica. This can be confirmed by comparing the SEM micrographs of the surfaces of the bituminous composites made with and

without the addition of the silica as presented in Figure 5a-g. These profiles suggest that the water absorption and swelling thickness can be fully believed with the presence of the structure of the silica and the low viscosity of the bituminous composite sample. This result also indicates that the water absorption and swelling thickness of the samples can be adjusted by regulating the formation of the silica, which is very useful to adjust the suitability of the material for the desired applications. Other factors governing the water absorption and swelling thickness may be the homogeneity of the composites, which is presented by SEM images of the sample surface (Figures 5e-g).

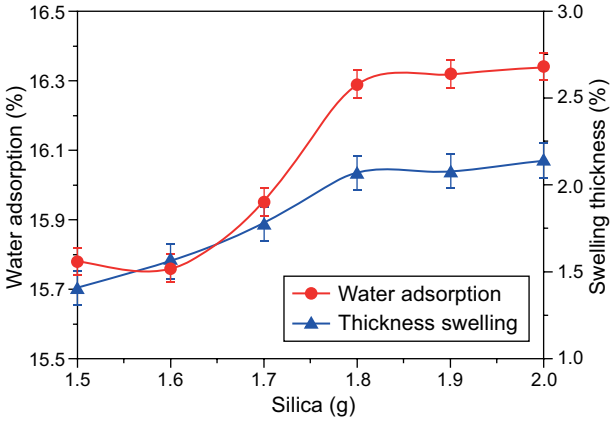

Figure 8. Variation in the water absorption and thickness swelling of the samples with the different silica additions.

CONLUSIONS

From the series of experiments conducted in this study, some conclusions were obtained regarding the analysis of the bituminous composite characteristics. The XRD study revealed the main structures are silica and amorphous carbon, which were associated with the silanol and C–H functional groups according to the FTIR analysis. The surface morphology of the bitumen without the silica addition presents a cluster of larger size than those with the addition of the silica. Also, the SEM analysis with the addition of the silica clearly indicates that the scattered silica covering the bituminous with a small grain size found in the bitumen ratio to silica is 1:2. The DTA/TGA analyses found that the temperature decomposition increased with the increase in the silica addition. In addition, an increased silica addition was followed by an increase in density, compressive strength, swelling thickness, and water absorption, while the opposite was true for the porosity. Therefore, it was found that the bituminous composite with a ratio of 1:2 is suitable for the design of roofing materials with increased compressive strength. Based on these characteristics, the samples are considered for a roofing material, suggesting their potential use in substitute lightweight steel roof devices.

Acknowledgements

The authors wish to thank and appreciate the Ministry of Research, Technology, and High Education, the Directorate General of Strengthening Research and Development, the Republic of Indonesia for the research funding provided through Hibah Competence Research Grant Batch I No: 062/SP2H/LT/DRPM/2019 Program in 2019

REFERENCES

1. Amutha K., Ravibaskar R and Sivakumar G. (2010): Extraction, Synthesis and Characterization of Nanosilica from Rice Husk Ash. *International nano Technology and Applied*, *4(1),* 61-66.
2. Haslinawati M. M., Matori K. A, Wahab Z. A, Sidek H..A. A., Zainal A. T. (2009): Effect of Temperature on Ceramic from Rice Husk Ash. *International Basic & Applied Science*, *09(09)*, 22-25.
3. Rafiee1 E., Shahebrahimi S., Feyzi1 M., and Shaterzadeh M. (2012): Optimization of synthesis and characterization of nanosilica produced from rice husk (a common waste material*). International Nano Letter*, *2(1)*, 1-8. doi:10.1186/2228-5326-2-29
4. Ugheoke B. I., and Mamat O. A. (2012): Novel method for high volume production of nano silica from rice husk: process development and product characteristics. *International Material Engineering Innovation*, *3(2)*, 139-155.
5. Faizul C. P., Abdullah C., and Fazlul B. (2013): Review of Extraction of Silica from Agricultural Wastes using Acid Leaching Treatment. *Advanced Material Research, 626*, 997-1000. doi:10.4028/www.scientific.net/AMR.626.997
6. Patil R., Dongre R., and Meshram J. (2014): Preparation of silica powder from rice husk. *Applied Chemistry, 27*, 26-29.
7. Hassan A. F., Abdelghny A. M., Elhadidy H., Youssef A. M. (2014): Synthesis and characterization of high surface area nanosilica from rice husk ash by surfactant-free sol-gel method. *Sol-Gel Science and Technology, 69*, 465-472. doi: 10.1007/s10971-013-3245-9
8. Tuan L. N. A., Dung L. T. K., Ha L. D. T., Hien N. Q., Phu D. V., Du B. D. (2017): Preparation and characterization of nanosilica from rice husk ash by chemical treatment combined with calcination. *Vietnam Journal of Chemistry*, *55(4)*, 446-455. doi: 10.15625/2525-2321.2017-00490
9. Liou T. H and Yang C. C. (2011): Synthesis and surface characteristics of nanosilica produced from alkali-extracted rice husk ash. *Material Science Engineering, B 17*6, 521-529. doi:10.1016/j.mseb.2011.01.007
10. Carmona, V. B., Oliveira R.M., Silva W. T. L., Mattoso L. H. C., and Marconcini J. M. (2013): Nanosilica from rice husk: Extraction and characterization. *Industry Crops and Production*, *43*, 291-296. doi:10.1016/j.indcrop.2012.06.050
11. Mohamed M. M., Zidan F. I., and Thabet M. (2008): Synthesis of ZSM-5 zeolite from rice husk ash: characterization and implications for photocatalytic degradation catalysts. *Micro and MesoMaterial*, *108(1-3),* 193-203. Doi: 10.1016/j.micromeso.2007.03.043.
12. Zahra G., and Habibollah Y. (2011): Preparation and Characterization of Nanozeolite NaA from Rice Husk at Room

Temperature without Organic Additives. *Nano Material*, 858961, 1-8. doi:10.1155/2011/858961

13. Serra M. F., Conconia M. S., Gaunaa M. R., Suáreza G., Aglietti E. F., Rendtorff N. M. (2016): Mullite ($3Al_2O_3 \cdot 2SiO_2$) ceramics obtained by reaction sintering of rice husk ash and alumina, phase evolution, sintering and microstructure. *Asian of Ceramic Society*, *4(1)*, 61-77. doi:10.1016/j.jascer.2015.11.003
14. Sembiring S., Simanjuntak W., Manurung P., Asmi D., and Low I. M. (2014): Synthesis and characterisation of gel-derived mullite precursors from rice husk silica. *Ceramic International*, *40(5)*, 7067-7072. doi:10.1016/j.ceramint.2013.12.038
15. Hossain S. K. S, Mathur L., Singh P., Majhi M. R. (2017): Preparation of forsterite refractory using highly abundant amorphous rice husk silica for thermal insulation. *Asian of Ceramic Society, 5*, 82-87. doi:10.1016/j.jascer.2017.01.001
16. Sembiring S., Riyanto A., Simanjuntak W., and Situmeang R. (2017): Effect of MgO–SiO_2 Ratio on the Forsterite (Mg_2SiO_4) Precursors Characteristics Derived from Amorphous Rice Husk Silica. *Journal of Oriental Chemistry, 33(4*), 1828-1836. doi:10.13005/ojc/330427
17. Andreola F., Martín M. I., Ferrari A. M., Lancellotti I., Bondioli F., Rincón J. M., Romero M., Barbieri L. (2013): Technological properties of glass-ceramic tiles obtained using rice husk ash as silica precursor. *Ceramic International, 39(5)*, 5427-5435. Doi:10.1016/j.ceramint.2012.12.050
18. Sembiring S., Simanjuntak W., Situmeang R., Riyanto A., and Sebayang K. (2016): Preparation of Refractory Cordieirite Using Amorphous Rice Husk Silica for Thermal Insulation Purposes. *Ceramic International, 42(7)*, 8431-8437. Doi:10.1016/j.ceramint.2016.02.062
19. Sarsam S. (2013): Improving Asphalt Cement Properties by Digestion with Nano Materials. Research and Application of Material (RAM), *Sciknow Publications Ltd. USA,1(6),* 61-64. doi:10.12966/ram.09.01.2013
20. Sarsam S. (2015): Impact of Nano Materials on Rheological and Physical Properties of Asphalt Cement. *International Journal of Advanced Material Research, 1(1)*, 8-14.
21. Mojtaba G., Morteza M. S., Majid T., Jalal K. R., Reza T. (2012): Modification of Stone Matrix Asphalt with Nano-SiO_2. *Journal of Basic Applied Science Research, 2(2)*, 1338-1344.
22. Ezzat H., El-Badawy S., Gabr A., El-Saaid Ibrahim Z., Breakah T. (2016): Evaluation of Asphalt Binders Modified with Nanoclay and Nanosilica. *Procedia Engineering, 143*, 1260-1267. doi:10.1016/j.proeng.2016.06.119
23. Yao H., You Z., Li L., Lee C. H., Wingard D., Yap Y. K., Shi X., Goh S. W. (2013): Rheological properties and chemical bonding of asphalt modified with nanosilica. *Journal of MaterialCivil Engineering, 25*(11), 1619-1630. doi:10.1061/(ASCE)MT.

1943-5533.0000690

24. You Z., Mills-Beale J., Foley J. M., Roy S. (2011): Nanoclay-modified asphalt materials: Preparation and characterization. *Construction Building Material, 25*(2), 1072-1078. doi: 10.1016/j.conbuildmat.2010.06.070
25. Shi X., Goh S. W., Akin M., Stevens S. (2012): Exploring the interactions of chloride deicer solutions with nanomodified and micromodified asphalt mixtures using artificial neural networks. *Material Civil Engineering, 24*(7), 805-815. doi: 10.1061/(ASCE)MT.1943-5533.0000452
26. Huang J., Yuro R., and Romeo G. A. (1995): Photooxidation of Corbett fractions of asphalt. *Fuel Science and Technology, 13*, 1121-1134. doi:10.1080/08843759508947727
27. Petersen J. C. (1998): A dual, sequential mechanism for the oxidation of petroleum asphalts. *Petroleum Science and Technology,* 16, 1023-1059. doi: 10.1080/10916469808949823
28. Yildirim Y. (2007): Polymer modified asphalt binders. *Construction Building Material, 21*(1), 66-72. doi:10.1016/j.conbuildmat.2005.07.007
29. Peters S. (2010): Nanocellulose and microcellulose fibers for concrete. Transportation Research Record 2142, Transportation Research Board, Washington, DC, 25-28.
30. Nair N. R, Mathew N. M, Thomas S., Chatterjee P., Siddqui M. A. (1992): Physical and rheological characteristics of liquid natural rubber modified bitumen. *Journal of Applied Polymer Science*, 68, 53-61.
31. Fernando M .J, Nadarajah M. (1992): Use of natural rubber latex in road construction. Polymer modified asphalt binders. *American Society for Testing and Material, Philadelphia, USA.*
32. Zhang F., and Yu J. (2010): The research for high-performance SBR compound modified asphalt. *Construction and Building Materials, 24*(3), 410-418. doi:10.1016/j.conbuildmat.2009.10.003
33. Shen J., Amirkhanian S. N., Xiao F., Tang B. (2009): Influence of surface area and size of crumb rubber on high temperature properties of crumb rubber modified binders. *Construction and Building Materials, 23*(1), 304-310. doi:10.1016/j.conbuildmat.2007.12.005
34. Cao W. (2007): Study on properties of recycled tire rubber modified asphalt mixtures using dry process. *Construction and Building Materials, 21*(5), 1011-1015. doi:10.1016/j.conbuildmat.2006.02.004
35. Putman B. J., and Amirkhanian S. N. (2004): Utilization of waste fibers in stone matrix asphalt mixtures. *Resource Conservation Recycle, 4*2(3), 265-274. doi: 10.1016/j.resconrec.2004.04.005
36. LeBaron P. C., Wang Z., Pinnavaia T. J. (1999): Polymer-layered silicate nanocomposites: an overview. *Applied Clay Science, 15*(1–2); 11-29. Doi:10.1016/S0169-1317(99)00017-4
37. Ray S. S., Okamoto M. (2003): Polymer/layered silicate nanocomposites: a review from preparation to processing. *Program Polymer Science, 28*(11); 1539-1641. doi: 10.1016/j.progpolymsci.2003.08.002
38. Wang H., Dang Z. X., Li L., and You Z. P. (2013): Analysis on fatigue crack growth laws for crumb rubber modified (CRM) asphalt mixture. *Construction and Building Materials, 47*, 1342-1349. doi:10.1016/j.conbuildmat.2013.06.014
39. Zhu J. Q., Birgisson B., and Kringos N. (2014): Polymer modification of bitumen: advances and challenges. *European Polymer, 54* (1), 18-38. doi: 10.1016/j.eurpolymj.2014.02.005
40. Lopes J. G., Correia J. R., and MacHado M. X. B. (2011): Dimensional stability of waterproofing bituminous sheets used in low slope roofs. *Construction and Building Materials, 25*(8), 3229-3235. doi: 10.1016/j.conbuildmat.2011. 03.009
41. Marques J. A., Lopes J. G., and Correia J. R. (2011): Durability of the adhesion between bituminous coatings and self-protection mineral granules of waterproofing membranes. *Construction Building Material, 25*(1), 138-144. doi:10.1016/j.conbuildmat.2010.06.047

42. Ping L., and Yunlong L. (2014): Review on Nano Modified Asphalt. *Applied Mechanics and Material*, *587*, 1220-1223. doi: 10.4028/www.scientific.net/AMM.587-589.1220
43. Australian Standard, Refractories and Refractory Material Physical Test Methods (1989): The Determination of Density, Porosity and Water Adsorption, Australian Standard (1-4); 1774.
44. JIS A 5908. (2003): Japanese Standard Association. Japanesse Industrial Standard Particle Board JIS A 5908. Japanese Standard Association.
45. Hesp S. A. M., Serban I., Shirokoff J. W. (2007): Reversible aging in asphalt binders. *Energy Fuels, 21*, 1112-1121. Doi**:** 10.1021/ef060463b
46. Yoo P. J and Yun T. (2013): Micro-heterogeneous modification of an asphalt binder using a dimethylphenol and high-impact polystyrene solution. *Construction and Building Materials, 49*, 77-83. doi: 10.1016/j.conbuildmat.2013.08.009
47. Bouhadda Y., Bormann, D., Sheu E., Bendedouch, D., Krallafa, A., Daaou, M. (2007): Characterization of Algerian Hassi-Messaoud asphaltene structure using Raman spectroscopy and x-ray diffraction. *Fuel*, *86*, 1855-64 doi:10.1016/j.fuel.2006.12.006
48. Siddiqui, M. N.; Ali, M. F.; Shirokoff, J. W. (2002): Use of x-ray diffraction patterns in assessing the aging pattern of asphalt fractions. *Fuel*, *81(1)*, 51-58. doi:10.1016/S0016-2361(01)00116-8
49. Babu, V. S., Seehra, M. S. (1996): Modeling of disorder and X-ray diffraction in coal-based graphitic carbons. *Carbon, 34(10)*, 1259-1265. doi:10.1016/0008-6223(96)00085-1
50. Zhang F., Yu J., Han J. (2011): Effects of thermal oxidative ageing on dynamic viscosity, TG/DTG, DTA and FTIR of SBS- and SBS/sulfur-modified asphalts. *Construction and Building Materials, 25*(1), 129-137. doi:10.1016/j.conbuildmat.2010.06.048
51. Adam F., and Chua J. H. (2004): The Adsorption of Palmytic Acid on Rice Husk Ash Chemically Modified with Al (III) Ion Using the Sol-gel Technique. *Journal of Colloid and Interface Science, 280*(1), 55-61. doi: 10.1016/j.jcis.2004.07.006
52. Tsai M. T. (2002): Effect of hydrolysis processing on the character of forsterite gel fibers Part II: "Crystallites and microstructural evolution. *Journal of Europen Ceramic Society, 22(7)*, 1085-1094. doi: 10.1016/S0955-2219(01)00418-6
53. Yao H., Dai Q., You Z. (2015): Fourier Transform Infrared Spectroscopy characterization of aging-related properties of original and nano-modified asphalt binders. *Construction Building Material, 101*(1), 1078-1087. doi: 10.1016/j.conbuildmat.2015.10.085
54. Ouyang C., Wang S., and Zhang Y. (2006): Improving the aging resistance of asphalt by addition of Zinc dialkyldithiophosphate. *Fuel, 85*(7-8), 1060-1066. doi: 10.1016/j.*fuel*.2005.08.023
55. Larsen D. O., Alessandrini J. L., Bosch A., and Cortizo M. S. (2009): Micro-structural and rheological characteristics of SBS-asphalt blends during their manufacturing. *Construction and Building Materials, 23*(8), 2769-2774. doi: 10.1016/j.conbuildmat.2009.03.008
56. Juan M., Jiménez M., Luis C. Q., Carmen R. (1996): Characterization of petroleum bitumens and their fractions by thermogravimetric analysis and differential scanning calorimetry. *Fuel, 75*, 1691-1700. doi: 10.1016/S0016-2361(96)00169-X